Signatures of possible surface states in TaAs

Nityan L. Nair,[1,2] Marie-Eve Boulanger [ORCID],[3] Francis Laliberté,[3] Sinead Griffin,[1,2] Sanyum Channa,[1,2] Anaelle Legros,[3,4]
Wojciech Tabis [ORCID],[5,6] Cyril Proust,[5,7] Jeffrey Neaton,[1,2] Louis Taillefer,[3,7] and James G. Analytis[1,2]

[1]*Department of Physics, University of California, Berkeley, California 94720, USA*
[2]*Materials Science Division, Lawrence Berkeley National Laboratory, Berkeley, California 94720, USA*
[3]*Institut Quantique, Département de Physique and RQMP, Université de Sherbrooke, Sherbrooke, Québec, Canada J1K 2R1*
[4]*Service de Physique de l'État Condensé (CEA, CNRS), Université Paris-Saclay, CEA Saclay, Gif-sur-Yvette 91191, France*
[5]*Laboratoire National des Champs Magnétiques Intenses (CNRS, EMFL, INSA, UJF, UPS), Toulouse 31400, France*
[6]*AGH University of Science and Technology, Faculty of Physics and Applied Computer Science, 30-059 Krakow, Poland*
[7]*Canadian Institute for Advanced Research, Toronto, Ontario, Canada M5G 1Z8*

We study Shubnikov–de Haas oscillations in single crystals of TaAs and find a previously undetected two-dimensional quantum oscillation that does not belong to the bulk Fermi surface. We cannot find an impurity phase consistent with our observations, and extensive diffraction measurements have not shown the presence of known impurity phases. We conjecture that the frequency originates from surface states that are sensitive to surface disorder. One candidate is the interference of coherent quasiparticles traversing two distinct Fermi arcs on the [001] crystallographic surface. The frequency and effective mass quantitatively agree with predictions of density functional theory and previous angle-resolved photoemission spectroscopy measurements of the Fermi arcs.

I. INTRODUCTION

Weyl semimetals host bulk carriers that behave not as massive electrons, but as massless chiral fermions. The topological nature of these charge carriers has led to many new emergent phenomena, including the presence of surface states known as Fermi arcs [1]. Although these are a necessary consequence of the existence of Weyl crossings, direct measurements of their transport properties remain rare as they are often masked by highly mobile bulk states. In fact, the transport contributions of Fermi arcs have been directly measured only in ultrathin samples of the Dirac semimetal Cd_3As_2 [2–4]. Recently, signatures of surface states were detected in NbAs [5], which, along with TaAs, was predicted and confirmed to be a Weyl semimetal [6,7]. While angle-resolved photoemission spectroscopy (ARPES) measurements have shown the presence of Fermi arc states on the surfaces of TaAs, as well as nontopological states originating from the surface termination, transport measurements have observed only quantum oscillations originating from bulk (three-dimensional) Fermi surfaces [8–12]. In this work, we report the observation of a set of Shubnikov de Haas (SdH) oscillations in high-quality crystals of TaAs and show that these oscillations can be attributed to coherent electron motion along the Fermi arcs of a Weyl semimetal. In contrast to the surface-bulk Weyl orbits expected in these systems and observed in Cd_3As_2, the observed oscillations appear to arise from the quantum interference of distinct Fermi arcs on a single-crystalline surface.

II. EXPERIMENT

High-quality single crystals of TaAs were grown using standard vapor transport techniques with iodine as the transport agent. Precursor powder was obtained by sealing a stoichiometric mixture of arsenic and tantalum powder in a quartz ampule under vacuum. The ampule was heated to 1100 °C and held for 4 days. The resulting powder was confirmed to be TaAs by powder x-ray diffraction. It was then mixed with 2.5 mg/cm^3 of iodine, sealed in a quartz ampule under vacuum, and loaded into a two-zone furnace. The source and sink ends of the furnace were held at 950 °C and 1050 °C, respectively, for 14 days. Well-faceted crystals up to 3 mm per side were obtained.

Single crystals of TaAs were ground into powder, and powder x-ray diffraction measurements were performed. The diffraction pattern is shown in Fig. 1. All the observed peaks can be indexed by TaAs, implying that there are no other crystalline phases present.

TaAs crystals were cut and polished into Hall bars with thicknesses ranging from 14 to 272 μm, with the main face normal to the [001] crystallographic axis. Transport measurements up to 14 T were performed in a Quantum Design physical property measurement system. Longitudinal and Hall resistivities (ρ_{xx} and ρ_{xy}) were measured using a standard five-contact lock-in measurement technique and symmetrized and antisymmetrized in field. High-field measurements were performed in Toulouse in pulsed fields up to 58 T. An ~10-kHz current excitation was applied to the sample, and high-speed acquisition was used to digitize the resulting voltage drop. The data were postanalyzed to perform a phase comparison and extract the resistivities. Results for the rise and fall of the field pulse were in good agreement.

In order to confirm crystallinity at the device level and eliminate the possibility that the Shubnikov–de Haas signal may be caused by impurity phases, local, spatially resolved Laue diffraction measurements were performed. Laue diffraction patterns were obtained using broadband x rays from the Advanced Light Source focused to a 1-μm spot. The spot was scanned across the sample to obtain spatially resolved
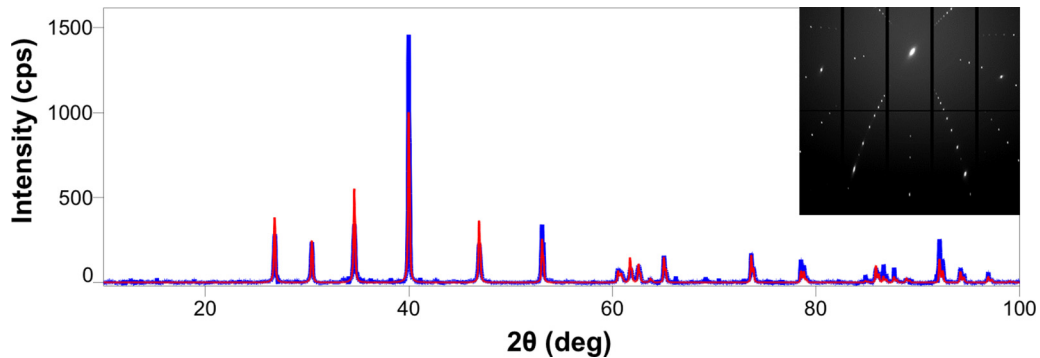
FIG. 1. The powder x-ray diffraction pattern from ground crystals of TaAs (blue) can be well fit by the calculated spectrum of TaAs (red). All observed peaks are accounted for, implying that additional phases are not present. Inset: The integrated intensity from 2500 Laue diffraction patterns taken over a $100 \times 100\,\mu m^2$ area of a TaAs Hall bar device. All the peaks can be well indexed by TaAs, and no indications of any impurity phases are present.

diffraction patterns. The observed peaks could be well indexed by TaAs, and no patterns corresponding to impurity phases were observed. The inset of Fig. 1 shows the summed diffraction image obtained from a $100 \times 100\,\mu m^2$ scan with a 2-μm step size of the active area of one of the transport devices exhibiting the 285-T oscillations. The image was generated by averaging 2500 individual Laue images. The peaks can be indexed by TaAs, and the lack of stray peaks indicates that no impurity phase is present over this $10\,000$-μm^2 area. A video showing the individual diffraction patterns can be found in Ref. [20].

Density functional calculations were performed with the Vienna Ab initio Simulation Package (VASP) code using the Perdew-Burke-Ernzerhof parametrization of the generalized gradient approximation, with spin-orbit coupling included self-consistently [13–15]. The projector augmented wave method is used for the electron-core interactions [16]. We expand the wave functions in plane waves to an energy cutoff of 600 eV. All calculations are performed at the experimental lattice parameters. To calculate the surface states and their spectrum, density functional theory (DFT) calculations of a slab consisting of seven unit cells (and terminated by As on one side and Ta on the other) are performed. To generate a Fermi surface associated with the surface states, we projected the slab eigenstates onto the first layer of the As-terminated surface and used dense k-grid sampling; Monkhorst-Pack k-point grids of $12 \times 12 \times 2$ and $400 \times 400 \times 1$ were used for slab self-consistent total-energy calculations and for slab Fermi surface calculations, respectively [17]. The computed Fermi surface associated with those states matches well with both previous slab calculations and ARPES studies [6,8]. The Fermi surface is computed with the PYPROCAR program [18]. We also generated a Fermi surface using a Wannier function and Green's function method, which agrees well with our slab calculation, albeit with a reduced band dispersion [19].

III. RESULTS

A. Transport and Shubnikov–de Haas effect

Figure 2 shows electrical transport measurements from one such device. At low temperature the resistivity reaches a value of 1 $\mu\Omega$ cm with a residual resistivity ratio of 56,

indicating the high crystal quality of the samples. Applying a magnetic field normal to the Hall bar reveals the large, nonsaturating magnetoresistance typical of these materials and pronounced SdH oscillations in both the longitudinal and Hall resistivities starting from fields below 1 T. Fourier analysis of these oscillations shows two principal frequencies: 7.3 T and 19.9 T. These values are in close agreement with frequencies previously reported for the bulk W1 and H1 Fermi pockets [12]. The angle dependence of these low-frequency oscillations [inset in Fig. 3(b)] can be attributed to the bulk Fermi surfaces of TaAs and is in quantitative agreement with previous studies [12]. This shows that the bulk properties of our samples are well understood and as expected. Upon subtraction of a high-temperature (10 K) background, however, an additional set of quantum oscillations can be observed that starts at $\sim$8 T and continues to high field. These oscillations have a frequency of 285 T; similar high-frequency oscillations have been observed in high-mobility nanoflakes of NbAs [5]. Such a large frequency is not expected to emerge from the small Fermi surfaces (either measured or calculated) of TaAs.

The dependence of the 285-T oscillation on field angle shows clear indications of a two-dimensional Fermi surface. Figure 3 shows the magnetoresistance as the field is tilted into the plane of the Hall bar. The derivative of ρ_{xy} is plotted to highlight the high-frequency oscillations. As the field is tilted into the plane of the device (from the [001] toward the [100] crystallographic direction), the 285-T frequency is observed to increase, and the onset of the oscillations moves to higher field. The frequency can be well fit by a $1/\cos(\theta)$ angle dependence, the hallmark of a two-dimensional Fermi surface. The two-dimensional nature of this surface has been confirmed in multiple devices and along multiple rotation directions [20].

The temperature dependence of the SdH oscillations is shown in Figs. 4(a) and 4(b). The amplitude can be fit to the Lifshitz-Kosevich form to extract the cyclotron effective mass for the different frequencies. The 7.3-T bulk frequency shows an effective mass of $0.066m_e$, in close agreement with the predicted value of $0.065m_e$ [12]. The 285-T frequency, on the other hand, shows a much larger effective mass of $0.5m_e$. This large mass is explained by a unique surface orbit involving
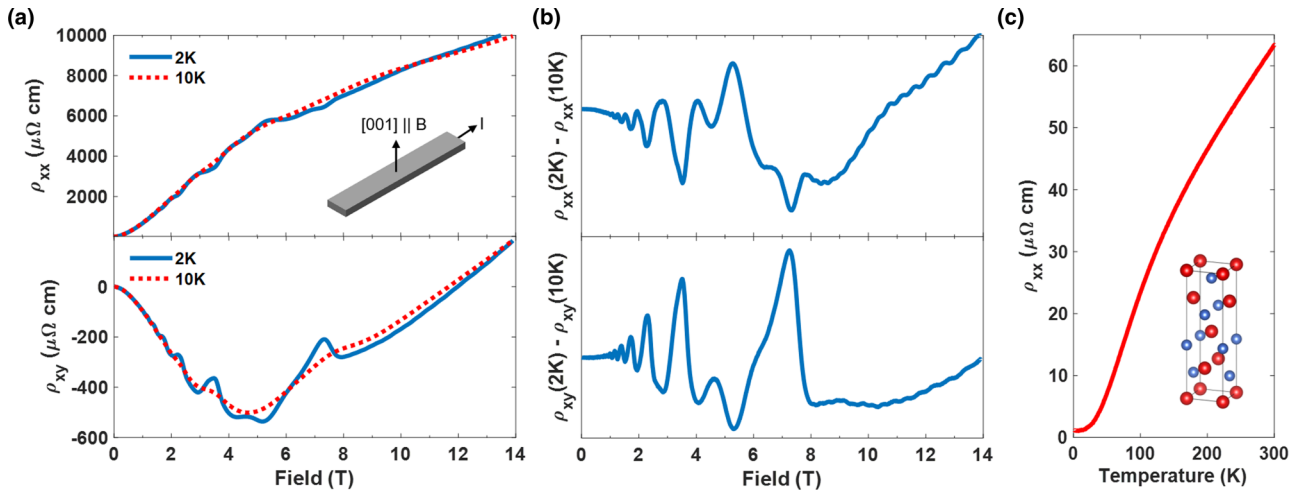
FIG. 2. A quantum oscillatory frequency in high-mobility TaAs. (a) The longitudinal magnetoresistivity (top) and Hall resistivity (bottom) of a polished 33-μm Hall bar device at 2 and 10 K with field applied along the [001] direction, normal to the device plane. SdH oscillations from the bulk Fermi surface are easily distinguishable. (b) The subtracted resistivities from (a). In addition to the bulk SdH oscillations, a high-frequency oscillation can be observed to start around 8 T with a frequency of 285 T. (c) The resistivity as a function of temperature, showing metallic behavior and a residual resistivity ratio of 56. Inset: The tetragonal crystal structure of TaAs. Ta atoms are shown in red, and As atoms are in blue.

the interference of two Fermi arcs on the [001] surface, as discussed below.

High-field measurements were also performed [Figs. 4(c) and 4(d)]. Interestingly, the frequency spectrum of the high-field oscillations appears to show a splitting [Fig. 4(d)]. Below 14 T, the oscillations appear to be periodic in inverse field with a frequency of approximately 285 T. Above 13 T, however, additional peaks emerge, and a beat pattern can be observed. This beating is responsible for the decrease in the oscillatory amplitude below approximately 0.1 T^{-1}. At lower fields this beat is not observable, so the amplitude always increases with field, as expected for the Lifshitz-Kosevich form [22].

A Fourier transform shows that two distinct frequencies, 287 and 274 T, can be resolved.

We note that our analysis of the quantum oscillatory phenomena is agnostic to their origin, discussion of which is left to Sec. IV.

B. Absence of oscillations in magnetic torque

Magnetic torque measurements were performed on a sample of TaAs. A crystal was polished to 33 μm, then cut into two pieces. One piece was used for magnetotransport measurements and is shown in Fig. 3. The other was used
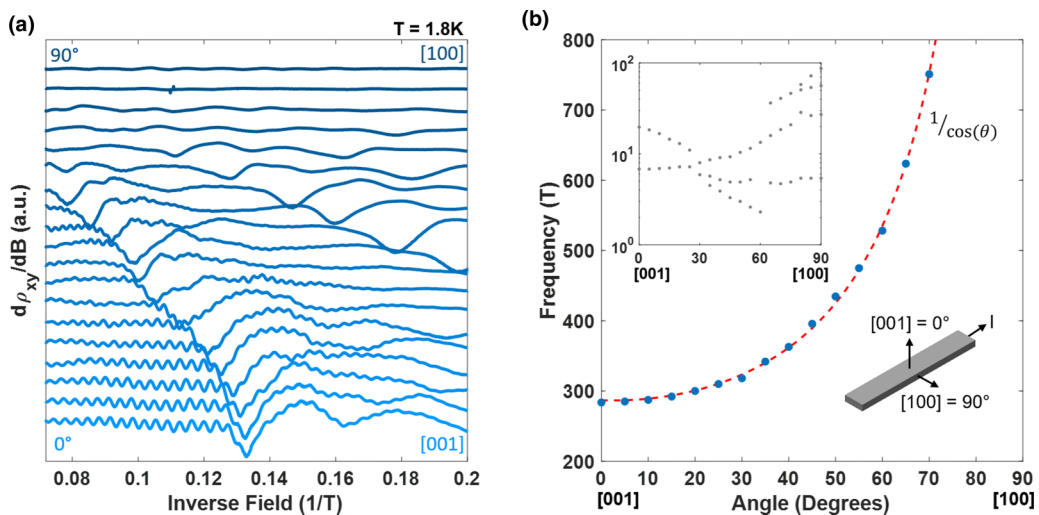

FIG. 3. The two-dimensional nature of the high-frequency quantum oscillations. (a) The derivative of the Hall resistivity plotted as a function of inverse magnetic field at different field angles. As the field is rotated into the plane of the Hall bar, the additional oscillation increases in frequency and moves to higher field. (b) The angle dependence of the oscillatory frequency shows the $1/\cos(\theta)$ dependence characteristic of a two-dimensional cyclotron orbit. Inset: The angle dependence of the low-frequency oscillations is in good agreement with what has been measured in bulk samples of TaAs [12].
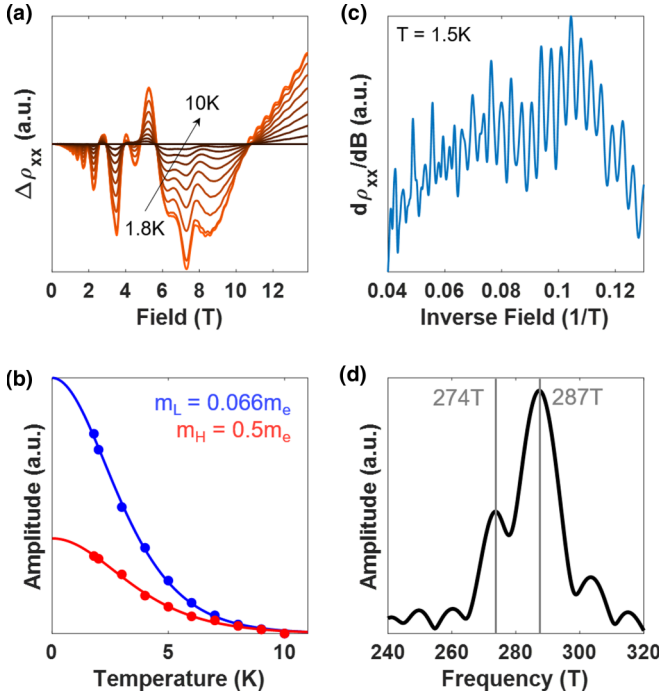
FIG. 4. Temperature and high field dependence. (a) Temperature dependence of the SdH oscillations with field along the [001] direction and a 10 K background subtraction. (b) The oscillatory amplitudes can be fit to the Lifshitz-Kosevich form to extract the cyclotron effective mass. The low-frequency bulk oscillations show an effective mass of $0.066m_e$, and the high-frequency 285-T oscillations show a much larger effective mass of $0.5m_e$. (c) The high-frequency SdH oscillations show an additional structure above 13 T. Beating of different frequencies, common in multiband systems, causes the oscillation amplitude to appear to decrease with increasing field. (d) A Fourier transform shows two frequencies emerging at 274 and 287 T, in close agreement with expectations of DFT (see Fig. 8).

for magnetic torque and is shown in Fig. 5. Although both samples were cut from the same polished crystal, the transport device clearly shows the 285-T oscillation and associated $1/\cos(\theta)$ dispersion. The torque device, on the other hand, does not show any indication of high-frequency oscillations.

This behavior is consistent with the oscillation originating from surface states in TaAs. Magnetic torque is sensitive to the total magnetization and therefore sensitive to the density of states on the surface of the device, which is small compared to the bulk. Transport, however, adds contributions of bulk and surface in parallel. In a parallel conductor model, such as the one applied in Sec. III C, a large magnetoresistance in one channel will cause more current to flow through the other channel, amplifying any changes in the resistance of the second channel. In this case, the bulk of TaAs is known to have a large magnetoresistance. This causes more current to flow on the surface, amplifying any oscillations in the surface resistivity. This oversampling of the surface states may explain why the oscillations are observed in transport but not torque.

C. Thickness-dependent measurements

In order to isolate whether the surface is playing a significant role in the transport, we studied the thickness
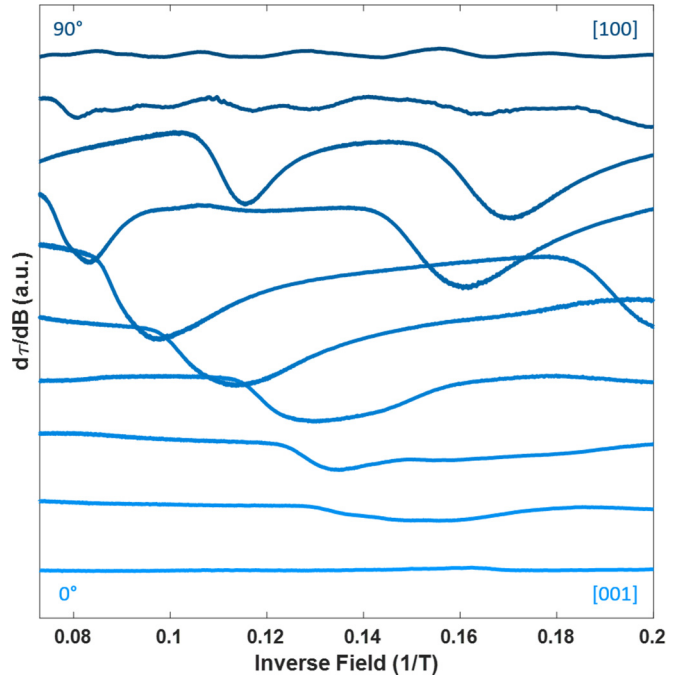

FIG. 5. The magnetic torque measured on a sample cut from the same crystal that was used in Fig. 3. There is no indication of the 285-T oscillation as field is rotated from the [001] axis to the [100] axis.

dependence of a single sample. A Hall bar device was sequentially polished to thicknesses of 272, 130, 43, and 14 μm. The magnetoresistivity exhibits a strong thickness dependence in both the resistivity and Hall channels, shown in Fig. 6, which immediately suggests there may be a surface contribution to the total conductance of the sample.

The complicated thickness dependence can be quantitatively understood using a parallel-channel model incorporating both bulk and surface contributions to the conductance. The conductivity tensor of each Fermi pocket (bulk electrons, bulk holes, surface electrons, and surface holes) is assumed to take the semiclassical form, given by

$$\sigma = \frac{n|e|\mu}{1+(\mu B)^2}\begin{bmatrix} 1 & \pm\mu B \\ \mp\mu B & 1 \end{bmatrix},$$

where n is the carrier density, e is the electron charge, μ is the carrier mobility, B is the applied magnetic field, and $\pm$ are for holes and electrons. We assume a partially compensated bulk consistent with what has been measured in TaAs by quantum oscillations and predicted by DFT with a Lifshitz-Kosevich oscillatory term added to simulate the 7.3-T oscillations of the W1 pocket [12,21,22]. The difference in scaling between the surface and bulk, stemming from their dimensionality, leads to a systematic change in the net carrier concentration as the sample is thinned, causing the Hall resistivity to decrease with sample thickness. This, in turn, changes the proportion of the current carried by the surface, leading to the complicated thickness dependence of the longitudinal magnetoresistance. Although this is a minimal model, the calculated resistivities (insets in Fig. 3) closely reproduce the features of the measured data using the parameters summarized in Table I.
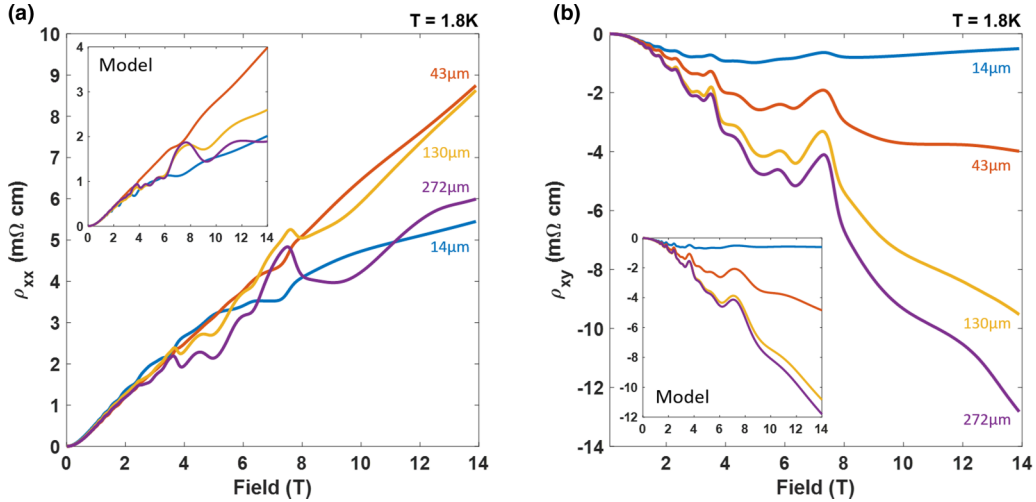
FIG. 6. Surface contribution to the conductivity. (a) Longitudinal and (b) Hall resistivities show a nontrivial thickness dependence. Resistivities were calculated using bulk geometrical factors. For a purely bulk conductivity, this would cause the curves to collapse. In addition, the SdH oscillations in the transverse magnetoresistivity appear to show a phase inversion between the 14 μm/43 μm devices and 130 μm/272 μm devices. Insets: The thickness dependence can be well modeled with a parallel-channel conductance model incorporating both surface and bulk contributions into device resistance. This model captures the overall shape and ordering of the resistivity curves and the phase inversion of the SdH oscillations. Temperature-dependent resistivities for each device are shown in Ref. [20]. Note field is always applied perpendicular to the current, so that extrinsic effects like current jetting are negligible.

Interestingly, the model accurately captures a curious feature in the bulk SdH signal: A phase inversion of the oscillations for thicknesses below 130 μm appearing in the ρ_{xx} channel but not the ρ_{xy} channel. The oscillation around 7 T, for example, appears as a peak in the longitudinal magnetoresistivities of the 272- and 130-μm devices but a trough in the 43- and 14-μm devices. In contrast, the same oscillation appears as a peak in the Hall resistivity for all thicknesses. This feature is well reproduced by the model. We note that a similar inversion of longitudinal magnetoresistivity oscillations with respect to the Hall resistivity has been observed in elemental bismuth and antimony and is understood as a competition between diagonal and off-diagonal terms of the conductivity tensor [23,24]. In TaAs, the larger influence of the surface in thinner devices changes the strength of the Hall conductance relative to the longitudinal magnetoconductance, leading to a similar phase inversion.

Our thickness-dependent measurements show that there is a large surface contribution to the total conductivity. The surface carrier densities obtained from DFT calculations (described in Sec. II; $\sim 2 \times 10^{15}$ cm^{-2} for both electrons and holes) are consistent with those determined from our simulations of the thickness dependence ($\sim 6 \times 10^{15}$ cm^{-2}). We note that the two-dimensional quantum oscillatory frequency we observe corresponds to $\sim 7 \times 10^{12}$ cm^{-2}, accounting for

only a small fraction of the total. Both trivial and topological (Fermi arc) surface states are present in this material. Most likely, the trivial states are not sufficiently mobile to allow coherent cyclotron orbits and associated SdH oscillations, although they contribute to the overall transport. In addition, as we argue below, the 285-T frequency likely arises from the difference of two Fermi surfaces and therefore will always appear to be smaller than the true Fermi surface.

We emphasize that that the parallel-channel model is underdetermined. To limit the number of free parameters, we have fixed bulk carrier densities to be consistent with known values [12] and have fixed the surface density and mobility to be constant as a function of thickness. The latter assumption is almost certainly inaccurate—given the aggressive nature of the polishing, there is good reason to believe that the surface parameters vary after each polishing step. Thus, the parallel-channel model establishes only that the presence of a surface channel of conduction is highly plausible, but the exact surface parameters given in Table I are probably accurate to only an order of magnitude.

Additionally, the surface oscillations show a complicated dependence on device thickness. In general, one would expect the surface oscillations to systematically grow in amplitude as the device thickness is reduced. This would be the case if all other material parameters were held constant. Unfortunately,

TABLE I. Parameters used to model the surface contribution to the conductivity of TaAs. Note that our model assumes the surface parameters are constant as a function of thickness (after each polishing step) and should therefore be considered to be only approximate.

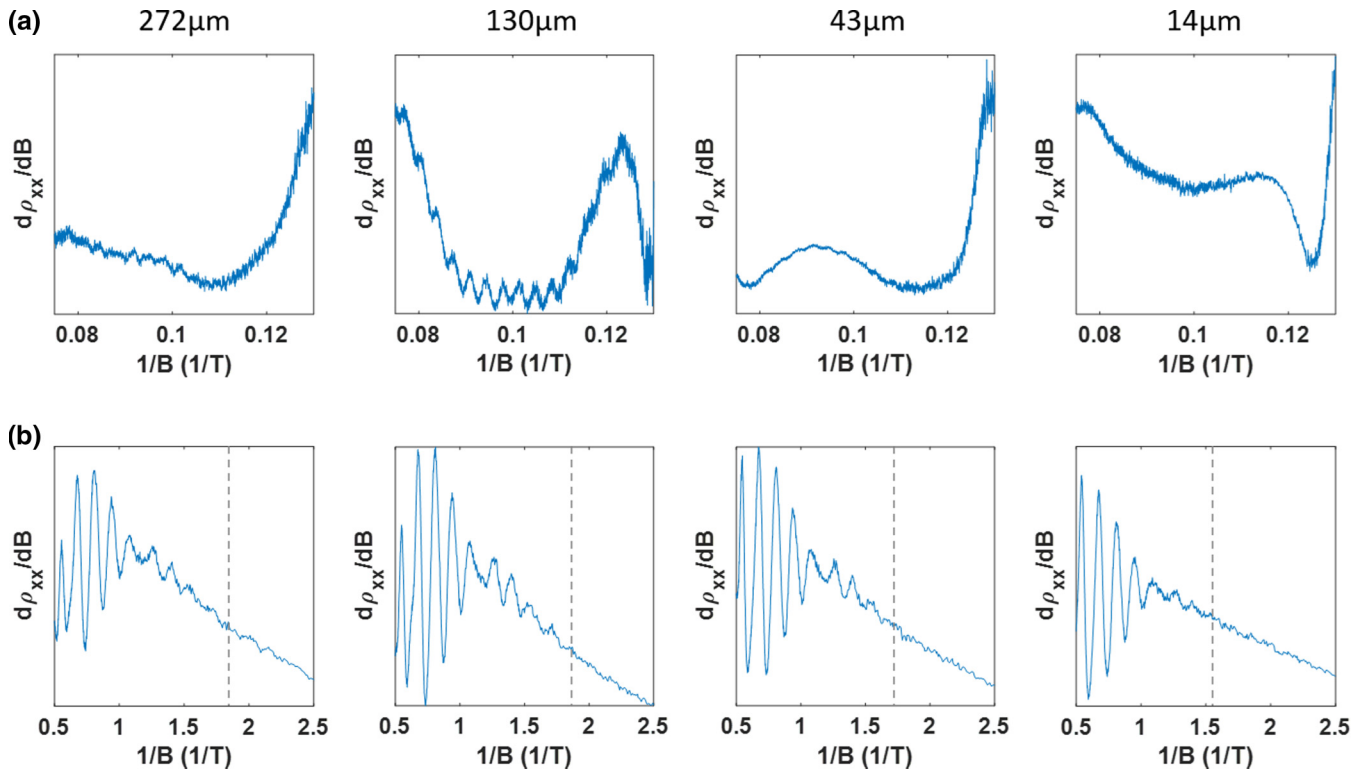|	Electron density	Hole density	Electron mobility (cm^2/V s)	Hole mobility (cm^2/V s)
Bulk	6.9×10^{18} cm^{-3}	6.2×10^{18} cm^{-3}	100 000	30 000
Surface	5.6×10^{15} cm^{-2}	6.1×10^{15} cm^{-2}	570	600

FIG. 7. (a) The thickness dependence of the 285-T oscillation appears to be nonmonotonic in device thickness. This may be the result of damaging the surface and reducing surface carrier mobility with subsequent polishing steps. (b) The bulk oscillations start at approximately the same field regardless of device thickness, indicating that the bulk mobility does not change significantly.

the methods used to polish the crystals are quite aggressive and involve mechanical abrasion, solvents, and multiple heating steps. As a result, surface disorder is likely being increased with every polishing step. This leads to a nonmonotonic dependence of the surface oscillations on device thickness, as shown in Fig. 7(a). For reference, the thickness dependence of the bulk oscillations is shown in Fig. 7(b). The oscillations begin at approximately the same field value regardless of sample thickness, indicating that the bulk mobility is not being changed by the polishing process. The fact that the low-frequency and high-frequency oscillations do not track with each other is evidence of their distinct origins, namely, the bulk and surface of the crystal.

D. Impurity considerations

Here, we consider the possibility that impurity phases in TaAs might lead to the observed high-frequency oscillations. The most likely impurity phases are elemental tantalum, elemental arsenic, and the binary compound $TaAs_2$. All three can be eliminated as the source of the observed oscillations: The known SdH frequencies are far from 285 T, their symmetries are inconsistent with the observed angle dependence, and they have effective masses that disagree with our observations [25–27].

Elemental tantalum shows quantum oscillations at much higher frequencies than what is observed in TaAs; the oscillations are higher than 2700 T for all field directions [25]. Tantalum can therefore be eliminated as the cause of the additional oscillations observed in TaAs.

Elemental arsenic, on the other hand, shows oscillations at much lower frequencies than tantalum [26]. The α and β Fermi surfaces both show oscillations at 285 T. However, there are three reasons why these surfaces can be eliminated as the cause of the oscillations observed. First, although arsenic shows oscillations at 285 T, it does so only for certain field angles. Both the α and β pockets have minima below 285 T, at 149 and 213 T, respectively. During extensive rotations of the field along different directions of the TaAs devices, the frequency of the oscillation was never found to drop below 285 T, incompatible with the arsenic Fermi pockets. Moreover, arsenic has a sixfold rotational symmetry in the x plane. This sixfold symmetry was not observed in the angle dependence of any of the TaAs devices, even for orthogonal rotation directions (see Ref. [20]). Last, the effective mass of the 285-T oscillations was measured to be $0.5m_e$ [see Figs 4(a) and 4(b)], much higher than the α and β pockets of arsenic at $0.098m_e$ and $0.13m_e$, respectively.

$TaAs_2$ also shows pronounced quantum oscillations from two principal pockets [27]. Like arsenic, however, these oscillations have minima significantly lower than the 285-T frequency observed. The α and β pockets are found to have frequencies of 104 and 130 T with field along the [001] axis, decreasing to 100 and 50 T, respectively, with rotation into the a-c plane. Moreover, the effective masses in $TaAs_2$ are found to be much lower than what was measured for the 285-T oscillation in TaAs, at $0.083m_e$ and $0.078m_e$. The appearance of one of these impurity phases on the surface, say, due to our polishing procedure, can similarly be ruled out. Moreover, extensive energy-dispersive

X-ray spectroscopy (EDX) did not show deviations from TaAs stoichiometry, suggesting intrusive surface phases are absent.

Another impurity possibility is the presence of small domains of a hexagonal structural phase of TaAs, which has been predicted to exist under pressure [28]. Although our samples are not measured under pressure, it is possible that the high-pressure phase could be stabilized as an impurity. The bulk Fermi surface of the hexagonal phase is predicted to consist of rings located at the K points. The cross-sectional area of these rings is found to correspond to a frequency of approximately 100 T, well below the minimum frequency we observe. Additionally, the sixfold symmetry expected for a hexagonal system is not observed.

It has been reported that planar defects, primarily in the form of stacking faults, can occur in crystals of TaAs [29]. Band structure calculations show these defects primarily change the location of the Fermi energy, appearing as an effective doping. The measured bulk quantum oscillation spectrum in our samples, however, agrees with what has been observed in the literature, implying that the Fermi energy in our materials is not significantly different from those measured previously. Moreover, one would expect defects, such as stacking faults, to be evenly distributed throughout the crystal. This would not result in a systematic thickness dependence of the magnetotransport, as observed in our Hall bar devices (see Fig. 6).

Finally, we note that the behavior of the 285-T frequency is very similar to the high-frequency oscillations ($F \sim 400$ T) recently reported in NbAs [5], which are also strongly two-dimensional. This suggests the frequencies have the same intrinsic origin.

IV. DISCUSSION

Previous ARPES studies together with our DFT calculations can help elucidate the origin of the surface oscillations [8]. Figure 8 shows a schematic of the electronic surface structure of the [001] As-terminated surface of TaAs. Although Weyl orbits involving individual Fermi arcs and traversing the bulk, as observed in Cd_3As_2, would be a natural explanation of the oscillations that we detect, the expected frequencies would be much higher than observed [2]. Moreover, coherent orbits from Fermi arcs on opposite surfaces require the traversal of the bulk, and since our samples are significantly thicker than the quantum mean free path ($\lambda \sim 0.1\,\mu$m), it seems highly unlikely that coherent orbits of this sort can form [30].

However, one orbit that matches our observations corresponds to the cyclotron path connecting two different Fermi arcs on a single surface, as illustrated in Fig. 8. Such an orbit involves an interband transition from one arc to another, a process known as magnetic breakdown that is observed in materials with nearly degenerate bands near the Fermi energy [22,31,32]. What is especially unusual about this orbit is that it is semiclassically forbidden; it involves electrons traveling opposite to the Lorentz force along one of the arcs. Such orbits are known to appear by Stark interference, the interference of two coherent cyclotron trajectories, and have been observed in magnesium and certain organic superconductors [33–35].
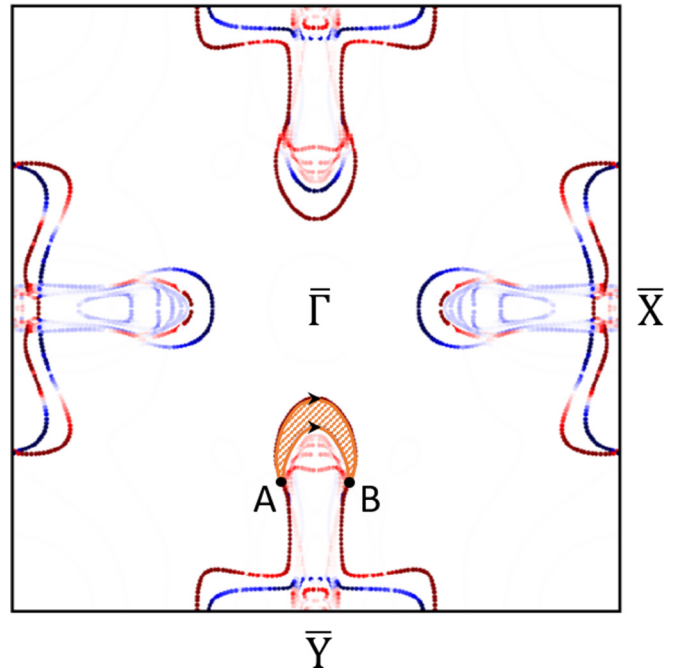

FIG. 8. Theoretical expectations of the quantum interference orbits. DFT calculation of the [001] Fermi surface of TaAs showing both trivial and Fermi arc surface states. The interference orbit between two Fermi arcs on the same surface is highlighted in orange. The area enclosed agrees closely with the SdH oscillation frequency observed in transport. The orbit near $\overline{X}$ is 7% larger than the equivalent orbit near $\overline{Y}$, in remarkable agreement with the frequency splitting we observe at high field [Fig. 4(d)].

In essence, the quantum-mechanical phase of the particles interferes as they are transmitted and reflected at the junctions where the arcs terminate.

To see that interference orbits can lead to quantum oscillations, consider a particle at position A in Fig. 8, at the left junction of the two arcs. If the particle travels to position B along the top or bottom arc, it will pick up an Aharonov-Bohm phase from the field enclosed by the associated real-space trajectory, $\phi = \frac{e}{\hbar} \int \mathbf{A} \cdot d\mathbf{l}$, where $\mathbf{A}$ is the vector potential. The phase difference between the two paths leads to interference of the wave function where the paths rejoin at point B. As a result, the total probability amplitude will be of the form $T \sim \cos(\phi_{\text{top}} - \phi_{\text{bottom}}) = \cos(\frac{e}{\hbar} \oint \mathbf{A} \cdot d\mathbf{l})$, where the integral is over the real-space path enclosed by the two Fermi arcs.

By Stokes's theorem, this path integral can be converted to a surface integral over the area enclosed, and the real-space area A_r can be converted into a k-space area A_k by $A_k = (\frac{eB}{\hbar})^2 A_r$. Therefore, as a result of the quantum interference of the paths, the probability amplitude becomes $T \sim \cos(\frac{\hbar A_k}{eB})$. This is of the exact same form as SdH oscillations with a frequency $F = \frac{\hbar A_k}{2\pi e}$, where A_k is now the area enclosed between the two Fermi arcs. A more detailed derivation is available in [36].

A_k estimated from ARPES measurements ($A_k \sim 0.026\,\text{Å}^{-2}$) is consistent with our DFT calculations and corresponds to a frequency of 277 T, in close agreement with the observed 285 T [8]. This places the Fermi level at about ~ 60 meV below E_F, even though the bulk Fermi

energy is ∼6 meV [12]. The difference can be explained by trivial band-bending effects at the surface, consistent with previous DFT calculations of the Fermi surface reported in [37,38]. Additionally, from different energy cuts, the cyclotron effective mass can be estimated by $m^* = \frac{\hbar^2}{2\pi}\frac{\partial A_k}{\partial \epsilon}$ and is found to be approximately $0.4m_e$, in reasonable agreement with the observed effective mass of $0.5m_e$. Given that no other surface or bulk states of TaAs, let alone known impurity phases, have masses close to this value, this agreement is strong verification that the observed frequency arises from the quantum interference of the Fermi arcs.

The observation of two distinct frequencies at high field also helps identify the origin as a Fermi arc interference orbit. The [001] surface of TaAs breaks the fourfold rotational symmetry of the crystal. As a result, the surface band structure does not have to be the same in the $\overline{X}$ and $\overline{Y}$ directions. In fact, the Fermi arcs connecting the W2 Weyl nodes are found to differ slightly in both DFT calculations and ARPES measurements [8]. This difference leads to an approximately 7% change in the area enclosed by the two quantum interference orbits, very close to the 5% splitting of the SdH frequencies observed in the present study.

Surface signatures of the Fermi arcs in Weyl and Dirac semimetals have proven to be extraordinarily difficult to detect, let alone find evidence of coherent orbits among them. The only system in which such orbits have been observed is Cd_3As_2, where the samples lend themselves to microfabrication techniques, allowing device thicknesses to approach the bulk mean free path. In TaAs, observation of these arcs is much more complicated; not only are there many more arcs that intersect in complex ways, but the material chemistry prevents the same microfabrication techniques from being used without significantly altering the surface [39]. In the present work, we have studied mechanically polished samples and revealed a SdH oscillation that sustains electron coherence along a cyclotron orbit. This orbit cannot be explained by any bulk Fermi surface or likely impurity phase. Using DFT calculations we have shown that this orbit quantitatively agrees with a cyclotron path involving the quantum interference of two Fermi arcs on the same surface. Interestingly, similar frequencies have been observed from surface states in high-mobility microflakes of NbAs, and even though cyclotron orbits in these flakes have comparably lighter masses, it would be interesting to see whether these orbits are consistent with this scenario [5]. These observations demonstrate that there are exciting possibilities not only to reveal the transport behavior of the Fermi arcs in high magnetic fields but to utilize field-driven interferometry as a means to study and employ their topological properties.

[1] X. Wan, A. M. Turner, A. Vishwanath, and S. Y. Savrasov, Phys. Rev. B **83**, 205101 (2011).

[2] P. J. W. Moll, N. L. Nair, T. Helm, A. C. Potter, I. Kimchi, A. Vishwanath, and J. G. Analytis, Nature (London) **535**, 266 (2016).

[3] G. Zheng, M. Wu, H. Zhang, W. Chu, W. Gao, J. Lu, Y. Han, J. Yang, H. Du, W. Ning, Y. Zhang, and M. Tian, Phys. Rev. B **96**, 121407(R) (2017).

[4] C. Zhang, A. Narayan, S. Lu, J. Zhang, H. Zhang, Z. Ni, X. Yuan, Y. Liu, J.-H. Park, E. Zhang *et al.*, Nat. Commun. **8**, 1272 (2017).

[5] C. Zhang, Z. Ni, J. Zhang, X. Yuan, Y. Liu, Y. Zou, Z. Liao, Y. Du, A. Narayan, H. Zhang *et al.*, Nat. Mater. **18**, 482 (2019).

[6] S. M. Huang, S. Y. Xu, I. Belopolski, C. C. Lee, G. Chang, B. Wang, N. Alidoust, G. Bian, M. Neupane, C. Zhang *et al.*, Nat. Commun. **6**, 7373 (2015).

[7] H. Weng, C. Fang, Z. Fang, B. A. Bernevig, and X. Dai, Phys. Rev. X **5**, 011029 (2015).

[8] L. X. Yang, Z. K. Liu, Y. Sun, H. Peng, H. F. Yang, T. Zhang, B. Zhou, Y. Zhang, Y. F. Guo, M. Rahn *et al.*, Nat. Phys. **11**, 728 (2015).

[9] S. Y. Xu, I. Belopolski, N. Alidoust, M. Neupane, G. Bian, C. Zhang, R. Sankar, G. Chang, Z. Yuan, C. C. Lee *et al.*, Science **349**, 613 (2015).

[10] B. Q. Lv, H. M. Weng, B. B. Fu, X. P. Wang, H. Miao, J. Ma, P. Richard, X. C. Huang, L. X. Zhao, G. F. Chen *et al.*, Phys. Rev. X **5**, 031013 (2015).

[11] B. Q. Lv, N. Xu, H. M. Weng, J. Z. Ma, P. Richard, X. C. Huang, L. X. Zhao, G. F. Chen, C. E. Matt, F. Bisti *et al.*, Nat. Phys. **11**, 724 (2015).

[12] F. Arnold, M. Naumann, S.-C. Wu, Y. Sun, M. Schmidt, H. Borrmann, C. Felser, B. Yan, and E. Hassinger, Phys. Rev. Lett. **117**, 146401 (2016).

[13] G. Kresse and J. Furthmüller, Phys. Rev. B **54**, 11169 (1996).

[14] G. Kresse and J. Hafner, Phys. Rev. B **47**, 558(R) (1993).

[15] J. P. Perdew, K. Burke, and M. Ernzerhof, Phys. Rev. Lett. **77**, 3865 (1996).

[16] G. Kresse and D. Joubert, Phys. Rev. B **59**, 1758 (1999).

[17] H. J. Monkhorst and J. D. Pack, Phys. Rev. B **13**, 5188 (1976).

[18] F. Munoz, U. Herath, and A. Romero, PYPROCAR: A PYTHON package for VASP and ABINIT postprocessing, https://github.com/uthpalah/PyProcar.

[19] Q. S. Wu, S. N. Zhang, H. F. Song, M. Troyer, and A. A. Soluyanov, Comput. Phys. Commun. **224**, 405 (2018).

[20] See Supplemental Material at http://link.aps.org/supplemental/10.1103/PhysRevB.102.075402 for data from additional samples, temperature dependent resistivities and extensive micro-Laue characterization of our devices.

[21] R. Sankar, G. Peramaiyan, I. P. Muthuselvam, S. Xu, M. Z. Hasan, and F. C. Chou, J. Phys.: Condens. Matter **30**, 015803 (2018).

[22] D. Shoenberg, *Magnetic Oscillations in Metals* (Cambridge University Press, Cambridge, 1984).

[23] M. Suzuki, H. Bando, and K. Oshima, Jpn. J. Appl. Phys. **20**, 1323 (1981).

[24] N. Satoh, Jpn. J. Appl. Phys. **37**, 161 (1998).

[25] M. H. Halloran, J. H. Condon, J. E. Graebner, J. E. Kunzier, and F. S. L. Hsu, Phys. Rev. B **1**, 366 (1970).

[26] M. G. Priestley, L. R. Windmiller, J. B. Ketterson, and Y. Eckstein, Phys. Rev. **154**, 671 (1967).

[27] Y. Luo, R. D. McDonald, P. F. S. Rosa, B. Scott, N. Wakeham, N. J. Ghimire, E. D. Bauer, J. D. Thompson, and F. Ronning, Sci. Rep. **6**, 27294 (2016).

[28] Y. Zhou, P. Lu, Y. Du, X. Zhu, G. Zhang, R. Zhang, D. Shao, X. Chen, X. Wang, M. Tian *et al.*, Phys. Rev. Lett. **117**, 146402 (2016).

[29] T. Besara, D. A. Rhodes, K.-W. Chen, S. Das, Q. R. Zhang, J. Sun, B. Zeng, Y. Xin, L. Balicas, R. E. Baumbach *et al.*, Phys. Rev. B **93**, 245152 (2016).

[30] A. C. Potter, I. Kimchi, and A. Vishwanath, Nat. Commun. **5**, 5161 (2014).

[31] M. H. Cohen and L. M. Falicov, Phys. Rev. Lett. **7**, 231 (1961).

[32] M. Kaganov and A. Slutskin, Phys. Rep. **98**, 189 (1983).

[33] R. W. Stark and C. B. Friedberg, J. Low Temp. Phys. **14**, 111 (1974).

[34] N. Harrison, J. Caulfield, J. Singleton, P. H. P. Reinders, F. Herlach, W. Hayes, M. Kurmoo, and P. Day, J. Phys.: Condens. Matter **8**, 5415 (1996).

[35] M. V. Kartsovnik, G. Y. Logvenov, T. Ishiguro, W. Biberacher, H. Anzai, and N. D. Kushch, Phys. Rev. Lett. **77**, 2530 (1996)

[36] M. V. Kartsovnik, Chem. Rev. **104**, 5737 (2004).

[37] A. Gyenis, H. Inoue, S. Jeon, B. B. Zhou, B. E. Feldman, Z. Wang, J. Li, S. Jiang, Q. D. Gibson, S. K. Kushwaha *et al.*, New J. Phys. **18**, 105003 (2016).

[38] H. Inoue, A. Gyenis, Z. Wang, J. Li, S. W. Oh, S. Jiang, N. Ni, B. A. Bernevig, and A. Yazdani, Science **351**, 1184 (2016).

[39] M. D. Bachmann, N. Nair, F. Flicker, R. Ilan, T. Meng, N. J. Ghimire, E. D. Bauer, F. Ronning, J. G. Analytis, and P. J. W. Moll, Sci. Adv. **3**, e1602983 (2017).